

Zero field precession and hysteretic threshold currents in spin torque oscillators with tilted polarizer

Yan Zhou, S. Bonetti, C. L. Zha, and Johan Akerman^y
Department of Microelectronics and Applied Physics,
Royal Institute of Technology, Electrum 229, 164 40 Kista, Sweden
(Dated: February 20, 2024)

Using non-linear system theory and numerical simulations we map out the static and dynamic phase diagram in zero applied field of a spin torque oscillator with a tilted polarizer (TP-STO). We find that for sufficiently large currents, even very small tilt angles ($\theta > 1^\circ$) will lead to steady free layer precession in zero field. Within a rather large range of tilt angles, $1^\circ < \theta < 19^\circ$, we find coexisting static states and hysteretic switching between these using only current. In a more narrow window ($1^\circ < \theta < 5^\circ$) one of the static states turns into a limit cycle (precession). The coexistence of static and dynamic states in zero magnetic field is unique to the tilted polarizer and leads to large hysteresis in the upper and lower threshold currents for TP-STO operation.

Spin torque, or the transfer of angular momentum from spin polarized electrons to magnetic moments [1, 2], currently receives an increasing interest due to potential use in magnetoresistive memory (MRAM) and in microwave signal generators, so-called spin torque oscillators (STO) [1, 2, 3, 4, 5, 6, 7, 8]. While the first spin torque devices were based on (pseudo-)spin valves with in-plane magnetizations, recent devices utilize perpendicularly magnetized layers to achieve both higher stability in MRAM and zero-field operation in STOs. The resulting static and dynamic phase diagrams have been studied in detail [9, 10, 11, 12].

In this Letter, we study the static and dynamic phase diagram of a spin valve where the magnetization of the fixed layer is tilted at an arbitrary angle out of the in-plane. This so-called Tilted Polarizer STO (TP-STO) has the significant advantage of zero-field operation while maintaining a high microwave output signal [13]. We here show, using non-linear system analysis, that the deviation from in-plane orientation creates a surprisingly rich phase diagram with coexistence of different static and dynamic states within a certain range of the polarizer tilt angle θ . We determine the stable precessional states using magnetodynamic macrospin simulations, and study the hysteretic switching between both different static states and between static and dynamic states. The coexistence of static and dynamic states in zero field is unique to the TP-STO and disappears for polarizer angles outside of $1^\circ < \theta < 19^\circ$. As a consequence, the TP-STO can exhibit unexpected large current-driven hysteresis in both the upper and lower threshold currents for precession.

Inset I in Fig. 1 shows the schematic structure of the TP-STO. While all films are deposited in the x-y plane, the fixed layer magnetization, \mathbf{M} , lies in the x-z plane, with an angle θ w.r.t. the x-axis. The time-evolution of the unit vector of the free layer magnetization $\hat{\mathbf{m}}$ is found from the Landau-Lifshitz-Gilbert-Slonczewski

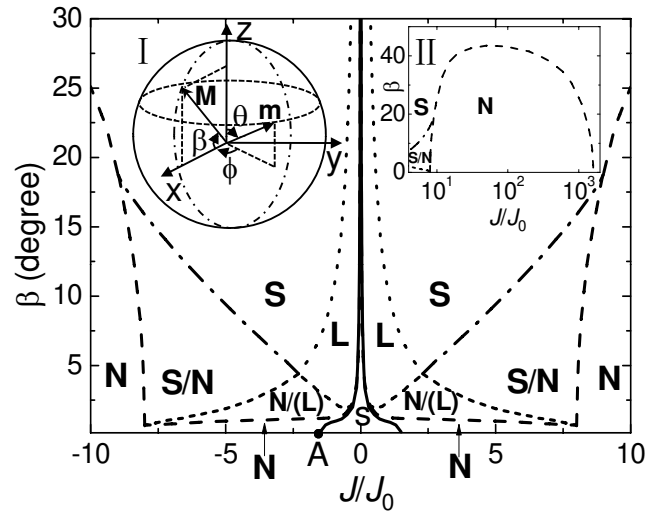


FIG. 1: Phase diagram of static and dynamic states of a TP-STO with nodes (N), spirals (S) and Limit cycles (L). Parentheses denote states only found through dynamical simulation. Inset I: The TP-STO structure: \mathbf{m} and \mathbf{M} are the magnetization vectors of free and fixed layer respectively. \mathbf{M} lies in the x-z plane with angle θ w.r.t. the x-axis, and θ and ϕ are the polar and azimuthal angles of the free layer magnetization \mathbf{m} . Inset II: Phase diagram of the high- J region.

(LLGS) equation [1, 2],

$$\frac{d\hat{\mathbf{m}}}{dt} = -\gamma \hat{\mathbf{m}} \times \mathbf{H}_{\text{eff}} + \frac{\alpha}{M} \hat{\mathbf{m}} \times \frac{d\hat{\mathbf{m}}}{dt} + \frac{\gamma}{M} \mathbf{j} \times \hat{\mathbf{m}} \times (\hat{\mathbf{m}} \times \hat{\mathbf{M}}); \quad (1)$$

where γ is the gyromagnetic ratio, α is the Gilbert damping parameter, and $\mathbf{j} = cJ$, with J being the electric current density and c a constant including material parameters and fundamental constants. The electric current is defined as positive when it flows from the fixed to the free layer and normalized by $J_0 = 10^8 \text{ A/cm}^2$. The effective field \mathbf{H}_{eff} carries the contribution of an anisotropy (easy axis) field H_k along the x-axis and a demagnetization (easy plane) field H_d . It should be noted that the applied magnetic field is set to zero throughout this Letter.

ter. For the results presented here, $j = 1.9 \cdot 10^3$ Hz/T, $\mu_0 H_d = 1$ T, $\mu_0 H_k = 10^2$ T, with μ_0 being the vacuum magnetic permeability. We use a symmetric torque term and a sinusoidal angular GMR dependence to not introduce further complications which would obscure the main results.

Eq. (1) can be transformed into the following set of differential equations in spherical coordinate system:

$$\begin{aligned} \dot{\theta} &= \frac{1}{2 + 1} (U + W); \\ \dot{\phi} &= \frac{1}{2 + 1} \frac{U - W}{\sin \theta}; \end{aligned} \quad (2)$$

with $U = H_k \cos \theta \sin^2 \phi + H_d \cos \theta \sin \phi \cos \phi$, and $W = H_k \cos \theta \sin \phi \sin \phi (\cos \phi \cos \phi \sin \phi \sin \phi)$.

By setting $(\dot{\theta}; \dot{\phi}) = 0$, we get a series of possible equilibrium solutions $\theta_i = \theta_i(\phi; J)$; $\phi_i = \phi_i(\theta; J)$, where $i = 1, \dots, i_t$ is the i th solution of total i_t solutions. However, these i_t equilibrium states are not all stable. We linearize Eq.(2) in the vicinity of $(\theta_i; \phi_i)$ and get:

$$\begin{pmatrix} \dot{\theta} \\ \dot{\phi} \end{pmatrix} = \begin{pmatrix} A(\theta_i; \phi_i) & B(\theta_i; \phi_i) \\ C(\theta_i; \phi_i) & D(\theta_i; \phi_i) \end{pmatrix} \begin{pmatrix} \delta\theta \\ \delta\phi \end{pmatrix}; \quad (3)$$

where A, B, C and D are the explicit functions of variables θ, ϕ and other material parameters. Following Ref. [14], the eigenvalues of the corresponding Jacobian, which determine the stability of the system, can therefore be solved and can always be expressed as: $\lambda_{1,2} = E(\theta_i; \phi_i) \pm F(\theta_i; \phi_i)$. For a solution to be stable, it must satisfy $\text{Re}(\lambda_{1,2}) < 0$. For real eigenvalues and $F > 0$, the eigenvalue with larger magnitude dominates and defines the only eigenvector governing the approach towards the final state, in this case a node (N). For $F = 0$ the two eigenvectors are identical and again define a node. For $F < 0$ the complex conjugate eigenvalues define two complex eigenvectors generating an oscillatory trajectory towards equilibrium, characteristic of a spiral-like (S) solution [15].

As an illustrating example, we show the procedure for determining the stability and type of solution for the case $\theta = 0$, i.e. for a conventional in-plane spin torque MRAM cell in zero field. The well known solution for negative current is $(\theta; \phi) = (0; 0)$, i.e. parallel alignment of the free and fixed layer magnetizations. Expanding Eq. (1) around this point yields:

$$\begin{pmatrix} \dot{\theta} \\ \dot{\phi} \end{pmatrix} = \begin{pmatrix} J(H_d + H_k) & H_k \\ H_d + H_k + J & H_k + J \end{pmatrix} \begin{pmatrix} \delta\theta \\ \delta\phi \end{pmatrix}; \quad (4)$$

with eigenvalues:

$$\lambda_{1,2} = \frac{H_d}{2} + \frac{J}{2} \pm \sqrt{\frac{H_d^2}{4} + H_k(H_k + H_d)(\theta^2 - 1) + f(\theta; \phi)}; \quad (5)$$

where $f(\theta; \phi) = J(H_d - 2H_k - J)$. By entering the parameters into Eq. (5), we see that the type of solution and its stability depend upon the value of J (i.e. J), if all other parameters are fixed. For $J = J_0$ $J < 1.5$ the solution is of spiral type (S), while outside this region, where the torque is larger, the solution is a node (N). Point A in Fig. 1 denotes the S ! N transition at negative currents. This result is well known in conventional spin torque switching where switching between S states proceeds by slow spiraling out of the unstable state and into the stable S state, while large currents will switch the magnetization without much precession into a stable N state [3].

Following this procedure, we now construct the static part of the phase diagram in Fig. 1 by finding all eigenvalues in the parameter space $0 < \theta < 90^\circ$ and $J = J_0$ $J < 1.6 \cdot 10^4$. While the entire parameter range was studied, Fig. 1 focuses on $0 < \theta < 30^\circ$ and $J = J_0$ $J < 10$, where coexistence of several different stable solutions are observed. It should be noted that only the static solutions (S and N) can be found from the eigenvalue analysis. To find the precessional states (L) we have to resort to numerical simulations below. However, according to the Poincare-Bendixson theorem [16, 17], the only possible final states of the system are either static states (fixed points) or limit-cycles (self-oscillation) and chaos is precluded since the free layer evolves on the unit sphere surface ($r = 1$) [18, 19]. In regions where there are neither S nor N solutions we can hence infer that steady precession (L) must take place.

For small enough J there is a single S state at all tilt angles θ , corresponding to the usual P/AP orientation of the free layer with respect to the in-plane projection of the fixed layer magnetization. For $\theta > 2^\circ$ this static state disappears with increasing current, and as discussed above, we can infer a precessional L state in this region. The crossover between S and L regions defines the critical current for the onset of precession (J_{c1}), where the negative damping from the spin polarized current destabilizes the S state and sustains continuous precession. It is hence possible to have zero-field TP-STO operation down to very small tilt angles if only large enough current densities can be realized. At yet smaller tilt angles (as in the in-plane case above) the eigenvalue analysis indicates that the S state changes into a node (N) with increasing current. It will however become apparent in the magnetodynamic simulations below that for $\theta > 1^\circ$ this region also contains a precessional state (hence the additional label (L)).

If the current is increased further, precession stops at an upper threshold current (J_{c2}) where the L state turns into a single spiral state located close to the north/south pole of the unit sphere. If we increase the current in the N=(L) region the same L ! S transition occurs but in addition, the node also remains stable. We hence observe a region S=N where two different stable static states co-

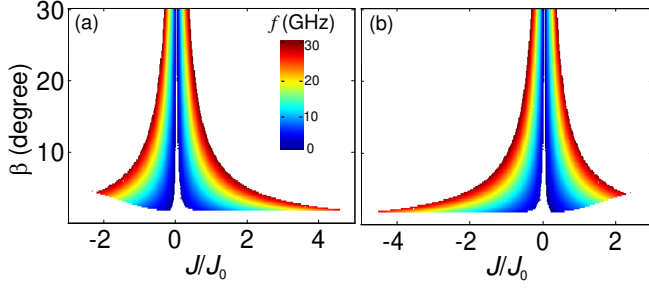


FIG. 2: Precession frequency f as a function of tilt angle and current swept from (a) negative to positive and (b) positive to negative. Inset: the onset critical current density for precession vs. β .

exist. The two states are located far from each other at two different points on the unit sphere: the north/south pole (S), and at P/AP alignment (N) respectively. As will become clear in the magnetodynamic simulation below, this separation allows both states to be realized by only sweeping the current.

Finally, at large currents (inset II of Fig. 1) there is a node state at P/AP alignment for $\beta < 40^\circ$ and a spiral state close to the north/south poles for $\beta > 40^\circ$. At extremely high currents, the S state gradually turns away from the poles, approaches P/AP orientation, and finally replaces the N state at about $J = J_0 > 10^3$ as the free layer magnetization aligns completely with the fixed layer. At these current densities ($J \sim 10^{11}$ A/cm²) any real sample would break down; we include this region for completeness.

To determine the dynamic states and also study the hysteretic switching between the coexisting static states, we now solve Eq. (1) using numerical simulation within the macro-spin approximation. To simulate actual hysteresis loops as a function of current, we start out at very large negative current, let the simulation reach a steady state, determine the type of state and its dynamic or static properties, and then let this state be the initial condition for the next simulation at the next current step. At very large negative (positive) currents, the free layer always aligns (anti-aligns) with the fixed layer, as was confirmed by a large set of random initial conditions. There is hence no dependence on the initial high-current state in our simulation.

The oscillation regions are shown in Fig. 2, for (a) increasing and (b) decreasing current and for the angular region of interest. The precession frequency varies from 0 to about 31 GHz. The critical current for the onset of magnetization precession depends strongly on the tilt angle β and is reduced almost two orders of magnitude when β increases from almost in-plane ($\beta = 2^\circ$) to perpendicular ($\beta = 90^\circ$). Both the trend and the quantitative values agree well with experiments and other simulations [9, 20, 21, 22].

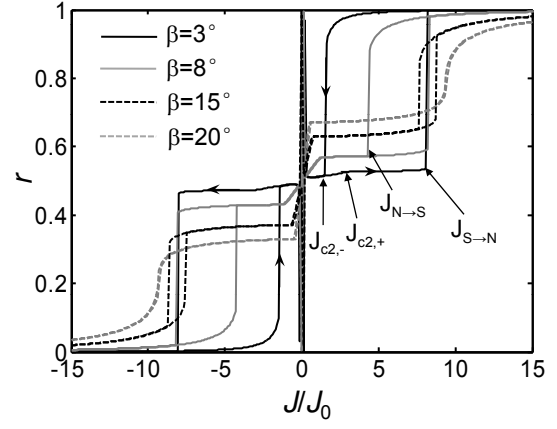


FIG. 3: Current-driven hysteresis loops for different $\beta = 3^\circ; 8^\circ; 15^\circ$ and 20° , showing large hysteresis in both the upper threshold current J_{c2} and the transition between the static S and N states.

One observes in Fig. 2 that the precession region is asymmetric and depends on the direction of the current sweep. In the low angle region, both the lower and upper threshold currents for precession exhibit hysteresis. We denote $j_{c1,+}$ and $j_{c2,+}$ as the lower and upper (absolute) threshold currents for increasing j , and similarly $j_{c1,-}$ and $j_{c2,-}$ as the corresponding currents for decreasing j . As seen in Fig. 2(a) $j_{c2,+}$ can be more than five times greater than $j_{c2,-}$ at small β . The hysteresis in J_{c1} is less obvious in Fig. 2, but will be discussed in detail in Fig. 4 at the end of the paper.

Using Fig. 2, we can now add information about the dynamical steady states and their boundaries to the phase diagram in Fig. 1. It is noteworthy that the boundaries in the two figures agree. Fig. 2 first confirms our assumption that the lack of a stable static state infers the existence of a limit cycle in the L region. Secondly, it adds a steady dynamic state to the region where our eigenvalue analysis only indicated N; we hence label this region $N = (L)$. While Fig. 2 indicates that this state only exists for $\beta > 2^\circ$, it does indeed extend all the way to the $N = (L) \rightarrow N$ boundary at about $\beta = 1^\circ$, as was confirmed by choosing initial conditions closer to precession. For $\beta > 2^\circ$ the S state at P/AP orientation must transform into L, but below $\beta = 2^\circ$ it can simply turn into the equivalent N state at P/AP orientation. Once in the N state there is no energetically favorable path to the L state. Finally, one realizes that the asymmetry in Fig. 2 stems from the selective realization of either the N or L state in the $N = (L)$ region. When approaching this region from above in a node state, the system stays in the node; if this region is approached from above in a spiral state, the system enters the dynamic precessional state L. To confirm this picture, we simulated minor loops where we limited the current sweep to remain in the S=N region before reversing the current direction. In this case the

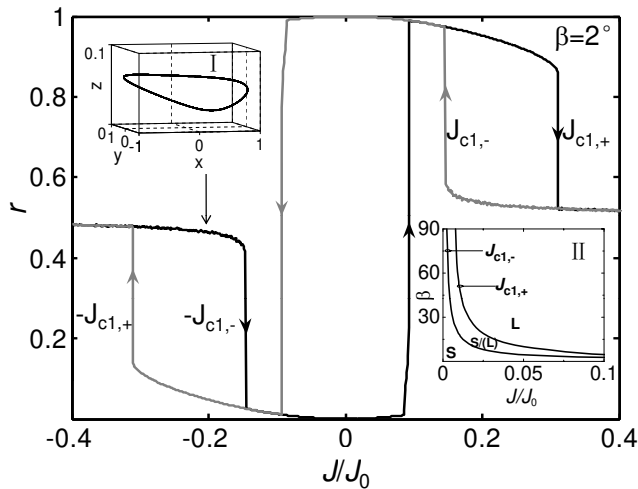


FIG. 4: Reduced MR vs. J for $\beta = 2^\circ$. Inset I shows the wide-angle orbit of the L state within the $S=(L)$ region. Inset II shows the angular dependence of the hysteretic threshold current J_{c1} .

high current N state is never realized and the S state again nucleates a precessional state already at the high value of $j_{c2,+}$ and not at the much lower $j_{c2,-}$.

Not only is the precessional state hysteretic, the two static states in the $S=N$ region also exhibit hysteresis. In Fig. 3 we plot the reduced magnetoresistance $r = (R - R_P)/(R_{AP} - R_P)$, where R_P and R_{AP} denote the resistance in the parallel and antiparallel configurations respectively, at four different polarizer angles. Close to $J = 0$ we observe the usual spin torque switching region between P and AP states. As the current is increased we first observe a linear r vs. J region at all angles characteristic of the average resistance within the precessional state L. As precession stops at $j_{c2,+}$, r reaches a plateau characteristic of the S state located close to the north/south poles. At a certain current value ($J_{S \rightarrow N}$), this state becomes unstable and m switches to its N state close to $P=AP$ alignment. If the current is again decreased, m stays within its N state well below $J_{S \rightarrow N}$ and only switches back at a much smaller current, either to an S state at $J_{N \rightarrow S}$ (> 5) or to an L state at $j_{c2,-}$ (< 5). At about $\beta = 20$, this hysteresis disappears and m rotates continuously $S \rightarrow N$.

We now turn to the hysteresis in the onset current of precession, J_{c1} . In Fig. 4 we plot r vs. J in the low- J region for $\beta = 2^\circ$. J_{c1} is clearly hysteretic with $j_{c1,+} \approx 0.3J_0$ and $j_{c1,-} \approx 0.15J_0$. For $0.15 < J/J_0 < 0.3$ the S type P/AP states hence coexist with a precessional L state with a very wide cone angle (inset I in Fig. 4). This hysteresis persists at all polarizer angles as shown in inset II in Fig. 4.

In conclusion, we have shown by non-linear system analysis and magnetodynamical simulations that a spin valve with a tilted fixed layer magnetization possesses

a surprisingly rich phase diagram of static and dynamic states in zero magnetic field. The coexistence of several of these states leads to a number of large hysteretic switching behaviors between both static and dynamic states and in particular to hysteresis in the threshold currents for magnetic precession.

We thank J. Persson for fruitful discussions. We gratefully acknowledge financial support from The Swedish Foundation for Strategic Research (SSF), The Swedish Research Council (VR), and the Goran Gustafsson Foundation. Johan Akerman is a Royal Swedish Academy of Sciences Research Fellow supported by a grant from the Knut and Alice Wallenberg Foundation.

Electronic address: zhouyan@kth.se

Electronic address: akerman1@kth.se

- [1] J. C. Slonczewski, J. Magn. Mater. 159, 1 (1996).
- [2] L. Berger, Phys. Rev. B 54, 9353 (1996).
- [3] J. Z. Sun, Phys. Rev. B 62, 570 (2000).
- [4] J. A. Katine, F. J. Albert, R. A. Buhrman, E. B. Myers, and D. C. Ralph, Phys. Rev. Lett. 84, 3149 (2000).
- [5] J. Grollier, V. Cros, H. Jarić, A. Hamzic, J. M. George, G. Faini, J. B. Youssef, H. Le Gall, and A. Fert, Phys. Rev. B 67, 174402 (2003).
- [6] S. I. Kiselev, J. C. Sankey, I. N. Kivorotov, N. C. Emley, M. Rinkoski, C. Perez, R. A. Buhrman, and D. C. Ralph, Phys. Rev. Lett. 93, 036601 (2004).
- [7] W. H. Rippard, M. R. Pufall, S. Kaka, T. J. Silva, and S. E. Russek, Phys. Rev. B 70, 100406(R) (2004).
- [8] Z. Li and S. Zhang, Phys. Rev. B 69, 134416 (2004).
- [9] D. Houshamdine, U. Ebels, B. Delaet, B. Rodmacq, I. Firastrau, F. Ponthenier, M. Brunet, C. Thirion, J.-P. Michel, L. P. Rebeau-Buda, M. C. Cyrille, O. Redon, and B. Dieny, Nat. Mater. 6, 447 (2007).
- [10] P. P. Horley, V. R. Vieira, P. M. Gorley, V. K. Dugaev, and J. Bamas, Phys. Rev. B 77, 094427 (2008).
- [11] U. Ebels, D. Houshamdine, I. Firastrau, D. Gusakova, C. Thirion, B. Dieny, and L. D. Buda-P. Rebeau, Phys. Rev. B 78, 024436 (2008).
- [12] I. Firastrau, D. Gusakova, D. Houshamdine, U. Ebels, M. C. Cyrille, B. Delaet, B. Dieny, O. Redon, J. C. Toussaint, and L. D. Buda-P. Rebeau, Phys. Rev. B 78, 024437 (2008).
- [13] Y. Zhou, C. L. Zha, S. Bonetti, J. Persson, and J. Akerman, Appl. Phys. Lett. 92, 262508 (2008).
- [14] Y. B. Bazaliy, B. A. Jones, and S. C. Zhang, Phys. Rev. B 69, 094421 (2004).
- [15] H. K. Khalil, Nonlinear Systems, third edition (Prentice Hall, Upper Saddle River, N.J., 2002).
- [16] J. H. Hubbard and B. H. West, Differential Equations: a Dynamical Systems Approach (Springer, Berlin, 1995).
- [17] L. Perko, Differential Equations and Dynamical Systems (Springer, Berlin, 1996).
- [18] G. Bertotti, C. Serpico, I. D. Mayergoyz, A. Magni, M. d'Aquino, and R. Bonin, Phys. Rev. Lett. 94, 127206 (2005).
- [19] X. Chen, Z. Zhu, Y. Jing, S. Dong, and J.-M. Liu, Phys. Rev. B 76, 054414 (2007).
- [20] J. Xiao, A. Zangwill, and M. D. Stiles, Phys. Rev. B 72,

- 014446 (2005).
- [21] K. J. Lee, O. Redon, and B. D. ieny, Appl Phys. Lett. 86, 022505 (2005).
- [22] F. B. M anco , N. D. R izzo, B. N. Engel, and S. Tehrani, Appl Phys. Lett. 88, 112507 (2006).